



## Article

# A Double-Electrode-Layer Wind-Driven Triboelectric Nanogenerator with Low Frictional Resistance and High Mechanical Energy Conversion Efficiency of 10.3%

Dongyang Fang, Guangqin Gu \*, Wenhe Zhang, Guangxiang Gu, Cong Wang, Bao Zhang, Gang Cheng \* and Zuliang Du

Key Lab for Special Functional Materials, Ministry of Education, National & Local Joint Engineering Research Center for High-Efficiency Display and Lighting Technology, School of Materials Science and Engineering, and Collaborative Innovation Center of Nano Functional Materials and Applications, Henan University, Kaifeng 475004, China

\* Correspondence: guguangqin@vip.henu.edu.cn (G.G.); chenggang@henu.edu.cn (G.C.)

**Abstract:** As a new technology for harvesting distributed energy, the triboelectric nanogenerator (TENG) has been widely used in harvesting wind energy. However, the wind-driven TENG (WD-TENG) faces the problems of high frictional resistance and low mechanical energy conversion efficiency. Here, based on optimizing the structure of the wind turbine, a rotational double-electrode-layer WD-TENG (DEL-WD-TENG) is developed. When the rotational speed is less than 400 round per minute (rpm), the dielectric triboelectric layer rubs with the inner electrode layer under its gravity; when the rotational speed is higher than 400 rpm, the dielectric triboelectric layer rubs with the outer electrode layer under the centrifugal force. The double-electrode-layer structure avoids the energy loss caused by other forces except gravity, centrifugal, and electrostatic adsorption, which improves the mechanical energy conversion efficiency and prolongs the working life of the DEL-WD-TENG. The conversion efficiency from mechanical energy to electricity of the DEL-WD-TENG can reach 10.3%. After 7 million cycles, the transferred charge of the DEL-WD-TENG is reduced by about 5.0%, and the mass loss of dielectric triboelectric layer is only 5.6%. The DEL-WD-TENG with low frictional resistance and high energy conversion efficiency has important application prospects in wind energy harvesting and self-powered sensing systems.

**Keywords:** triboelectric nanogenerator; wind energy harvesting; high mechanical energy conversion efficiency; low frictional resistance



**Citation:** Fang, D.; Gu, G.; Zhang, W.; Gu, G.; Wang, C.; Zhang, B.; Cheng, G.; Du, Z. A Double-Electrode-Layer Wind-Driven Triboelectric Nanogenerator with Low Frictional Resistance and High Mechanical Energy Conversion Efficiency of 10.3%. *Nanoenergy Adv.* **2023**, *3*, 236–246. <https://doi.org/10.3390/nanoenergyadv3030012>

Academic Editors: Christian Falconi, Sang Min Lee and Ya Yang

Received: 25 May 2023

Revised: 28 July 2023

Accepted: 1 August 2023

Published: 8 August 2023



**Copyright:** © 2023 by the authors. Licensee MDPI, Basel, Switzerland. This article is an open access article distributed under the terms and conditions of the Creative Commons Attribution (CC BY) license (<https://creativecommons.org/licenses/by/4.0/>).

## 1. Introduction

As a common source of renewable energy in daily life, the proportion of wind power in global electricity generation is steadily increasing. According to the report of Global Wind Energy Council (GWEC), wind power will account for 12% of global electricity generation by 2023 [1]. Wind turbines based on electromagnetic induction comprise the main technology of wind power generation. However, due to high cost, complex structure, heavy weight, and wind speed limits, the usage scenarios of wind turbines are limited to areas far from cities and buildings [2]. With the development of new generation information technology such as the Internet of Things, numerous and widely distributed sensors have a significant demand for distributed energy. Hence, it is of great importance to study new wind energy harvesting technologies and develop portable wind energy harvesters. Triboelectric nanogenerator (TENG), which can efficiently convert various forms of mechanical energy in the environment into electricity, was invented in 2012 [3]. With the advantages of simple preparation, low cost, wide material sources, multiple working modes, and high energy conversion efficiency at low frequencies, TENG is promising in wind energy harvesting and self-powered systems [4].

Up to now, wind-driven TENGs (WD-TENGs) consist mainly of rotating structure and flutter structure WD-TENGs. When the flutter structure WD-TENG collects wind energy, the wind blows the film to generate vibrations [5–16]. During the vibration process, the contact and separation movement between the dielectric triboelectric layer and the electrode is realized to generate current. The flutter structure WD-TENG is small in size and low in cost, but it has few application scenarios and a small working wind speed range. The rotating structure WD-TENG drives the rotor to realize the mutual friction motion between the dielectric triboelectric layer and the electrode through the rotation of the fan blades blown by the wind to generate current. Compared with the flutter structure WD-TENG, the rotating structure WD-TENG has the advantages of high output, high efficiency, high stability, long working life, and a wider speed range of wind collected. In recent years, a variety of rotating structure WD-TENGs have been developed [17–25]. In 2015, Li et al. reported a rotational WD-TENG that can complete free conversion between contact and non-contact modes [26]. At low rotational speeds, the WD-TENG works in a contact state to supplement triboelectric charge, and at high rotational speeds, the WD-TENG works in a non-contact state to reduce wear. In 2021, Chen et al. reported a soft contact rotating WD-TENG. Soft and density animal fur is used to reduce frictional loss and improve electrical output of WD-TENG [27]. In 2021, Yong et al. reported a self-powered system based on an auto-switching dual-rotating axis TENG that can efficiently collect wind energy over broadband wind speeds (2.2–16 m/s) [28]. Appropriate contact between arched protrusion and stator generated by the elasticity of dielectric triboelectric layer can reduce frictional resistance and abrasion. These works improved the output performance of WD-TENGs and broadened the range of wind energy collection, which is of great significance for promoting the application of WD-TENGs. However, they focused on the improvement of output performance and the reduction of abrasion. The reduction of frictional resistance brought by the external forces and the improvement of mechanical energy conversion efficiency are ignored. Hence, WD-TENGs with low frictional resistance, low abrasion, and high energy conversion efficiency should be developed.

Here, based on optimizing the structure and parameters of the wind turbine, a rotational double-electrode-layer WD-TENG (DEL-WD-TENG) is developed. The DEL-WD-TENG first selects the horizontal axis wind turbine with higher wind energy utilization rate as the wind energy collection device, and further improves the wind energy utilization rate by optimizing the number of blades. Secondly, it uses electrostatic adsorption force and centrifugal force to make the triboelectric layer adsorbed on the electrode. The main interaction between the electrode and the dielectric triboelectric layer is electrostatic adsorption force, which can effectively reduce the frictional resistance and abrasion, prolonging the working life and energy conversion efficiency of WD-TENG. Finally, a double-layer TENG structure is proposed so that the DEL-WD-TENG can work with most wind speeds. When the rotational speed is less than 400 round per minute (rpm), the triboelectric layer rubs with the inner electrode layer. When the rotational speed is higher than 400 rpm, the triboelectric layer rubs with the outer electrode layer under the action of centrifugal force. The efficiency of mechanical energy to electricity of DEL-WD-TENGs can reach 10.3%. After 7 million cycles, the transferred charge of the DEL-WD-TENG is reduced by about 5.0%, and the mass loss of the friction layer is only 5.6%. The DEL-WD-TENG with low frictional resistance and high energy conversion efficiency has important application prospects in wind energy harvesting and self-powered systems.

## 2. Results and Discussion

### 2.1. Energy Conversion Efficiency Calculation

The WD-TENG is mainly used to harvest wind energy from the surrounding environment and convert it into electricity. Wind energy in the natural environment generates rotational mechanical energy through the wind turbine, which is further converted into electric energy through the WD-TENG and ultimately powers the electronic devices, thus forming self-powered systems, as shown in Figure S1. Hence, there are two aspects to

improve the energy conversion efficiency from wind energy to electric energy. First, the number of wind turbine blades should be optimized to improve the energy conversion efficiency from wind energy to rotary mechanical energy. Second, the efficiency of mechanical energy to electricity is improved, thus improving the energy conversion efficiency of the WD-TENG.

According to the relative position of the rotating axis of the wind turbine and the ground, the wind turbine is divided into two types: horizontal and vertical axis wind turbines. Wind energy utilization coefficient  $C_p$  (the ratio of the energy of a wind turbine can obtain from the wind in a unit time) is used to evaluate the performance of a wind turbine, and the  $C_p$  of the horizontal-axis wind turbine is higher than that of the vertical axis wind turbine. The  $C_p$  of the horizontal-axis wind turbine can be further improved by optimizing the structure [29].

The mechanical energy conversion efficiency of WD-TENG is defined as the ratio of the electrical energy supplied to the load to the input mechanical energy, which can be expressed by the following Equation:

$$\eta = \frac{E_{output}}{E_{input}}, \quad (1)$$

where  $\eta$  is the energy conversion efficiency of TENG; and  $E_{output}$  and  $E_{input}$  are the output electrical energy and input mechanical energy, respectively. The specific equations are as follows:

$$E_{output} = \int_0^t I^2 R dt; \quad (2)$$

$$E_{input} = \int_0^t \frac{T \cdot N}{k} dt, \quad (3)$$

where  $R$  and  $I$  are external load resistance and current, respectively;  $T$  is the torque generated by rotational friction;  $N$  is the rotational speed; and  $k$  is a constant with a value of 9549.

Hence, to improve the energy conversion efficiency of the WD-TENG, it is necessary to optimize the structure of the wind turbine to increase the conversion efficiency of wind energy to rotary energy and reduce the frictional loss of the WD-TENG to improve the energy conversion efficiency of the TENG.

## 2.2. Optimization of Wind Turbines

A horizontal-axis wind turbine with higher  $C_p$  and lower starting wind speed is selected. Figure 1a shows a wind turbine with nine blades. By changing the number of blades ( $n = 3-9$ ), the rotational speed of different wind turbines at different wind speeds and the time taken by different wind turbines to reach the maximum rotational speed at the same wind speed are analyzed, respectively. Under the wind speed of 3.5 m/s, the rotational speed of the wind turbine increases with the increase in blade number, as shown in Figure 1b. As can be seen from Figure 1c,d, it takes a short time for the wind turbine with nine blades to reach the maximum speed, which has the highest rotational speed under different wind speeds. Therefore, the wind turbine with nine blades is selected. The influences of the rotor mass and windscreen area on rotational speed are shown in Figure 1e,f, respectively. Reducing the mass of the rotor and the windscreen area can further improve the rotational speed of the wind turbine at the same wind speed, thus improving the wind energy collection efficiency. Finally, a horizontal-axis wind turbine with nine blades and a weight of 90 g is used. The diameter of the WD-TENG is set as 100 mm.

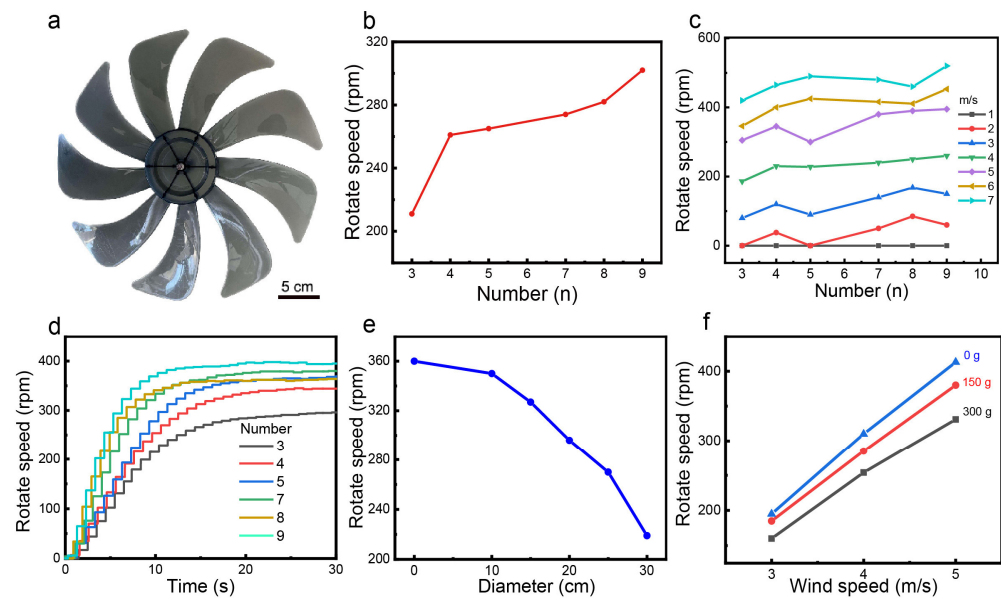


**Figure 1.** (a) Optical image of wind turbine blades. (b) Rotational speed with different numbers of wind turbine blades at the same wind speed. (c) Rotational speed of different wind turbine blades and different wind speeds. (d) Time of different wind turbine blades to reach maximum speed. (e) Rotational speed of rotors with different weights. (f) Influence of the windscreen area behind the wind turbine blade on the rotational speed.

### 2.3. Structure and Working Principle of DEL-TENG

A double-electrode-layer WD-TENG (DEL-WD-TENG) is designed in which the interactions between the dielectric triboelectric layer and the electrode are electrostatic adsorption and centrifugal force. Figure 2a shows the torque measurement system of the DEL-WD-TENG. The detailed structure of the DEL-WD-TENG is shown in Figure 2b, which is composed of a rotor, a polytetrafluoroethylene (PTFE) dielectric triboelectric layer, and a double-electrode-layer stator. The DEL-WD-TENG has a coaxial barrel structure. The PTFE layer is fixed on an acrylic rod of the rotor between the inner and outer electrode layers. The rotor is connected to the wind turbine and rotates, driven by the wind.

Rotational speed determines the working state of the DEL-WD-TENG. When the rotational speed is lower than 400 round per minute (rpm), the PTFE film rubs with the inner copper (Cu) electrode layer under its gravity, as shown in Figure 2c. As a brief description, it is called the inner WD-TENG. The electrostatic adsorption between the two triboelectric layers enables the PTFE film to be adsorbed on the inner Cu electrode, which makes effective contact and reduces the friction loss caused by other forces. When the rotational speed is higher than 400 rpm, the PTFE film is separated from the inner Cu layer due to the centrifugal force, as shown in Figure 2d. It is called the outer WD-TENG. Under the action of centrifugal force and electrostatic adsorption force, the PTFE film is attached to the outer Cu electrode. Therefore, the DEL-WD-TENG operates in different operating modes at different rotational speeds. The DEL-WD-TENG eliminates the mechanical energy loss caused by other forces except electrostatic adsorption and centrifugal force, which improves mechanical energy conversion efficiency and working life.

When the rotational speed is lower than 400 rpm, the working mechanism of the inner WD-TENG is shown in Figure 2c. After working for several cycles, due to the triboelectric effect, the Cu electrodes and PTFE films gain equal positive and negative charges, respectively [30]. When the PTFE films and Cu electrodes are in the position of Figure 2e<i>, the inner WD-TENG is in electrostatic equilibrium state, and there is no charge transfer between the two Cu electrodes. As the PTFE films slides toward Cu electrode 2, electrons flow from Cu electrode 2 to Cu electrode 1 due to potential difference, thus forming current on the external load, as shown in Figure 2e<ii>. When the PTFE

films is fully attached to Cu electrode 2, the inner WD-TENG achieves another electrostatic equilibrium state, as shown in Figure 2c<iii>. As shown in Figure 2e<iv>, when the PTFE film gradually slides to Cu electrode 1, electrons will flow from Cu electrode 1 to Cu electrode 2, creating a current in the opposite direction in the external circuit. When the PTFE film is separated from Cu electrode 2 again, one charge transfer cycle is completed. Due to the same structure and working mode, the working mechanism of the DEL-WD-TENG when rotational speed is higher than 400 rpm is the same, as shown in Figure S2. Even if the PTFE films slide in the opposite direction, the working mechanism is also the same, but the current is in the opposite direction.

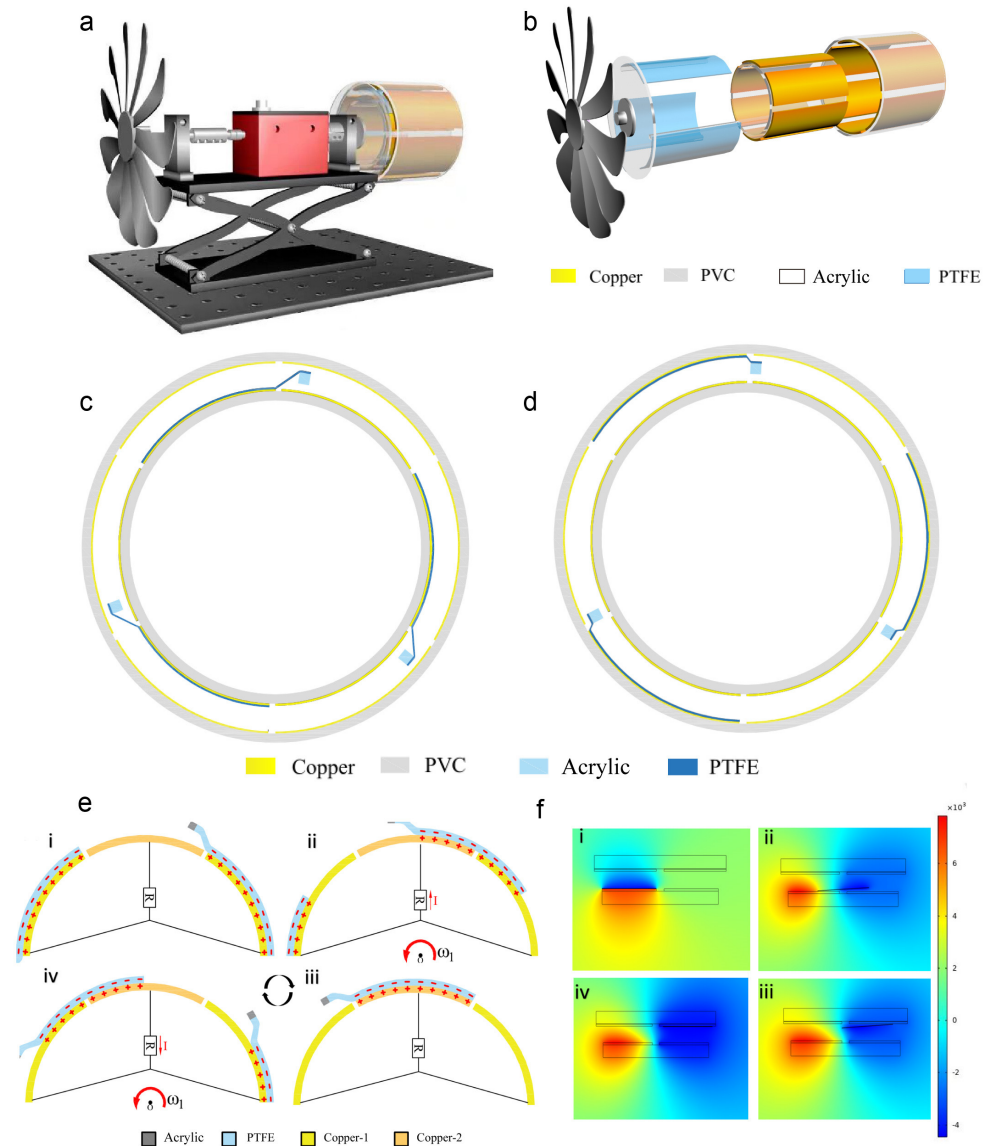


**Figure 2.** (a) Schematic diagram of torque measurement system. (b) Schematic diagram of the DEL-WD-TENG split structure. Schematic diagram of the working mechanism of the DEL-WD-TENG when the rotational speed is lower than 400 rpm (c) and higher than 400 rpm (d). (e) Working mechanism of the DEL-WD-TENG when the rotational speed is lower than 400 rpm: <i> static equilibrium state, fully overlapping position; <ii> intermediate state, PTFE film is sliding apart; <iii> another static equilibrium state, fully overlapping position; <iv> another intermediate state, PTFE film is sliding apart. (f) Potential simulation of four working states: <i> static equilibrium state, fully overlapping position; <ii> intermediate state, PTFE film is sliding apart the inner Cu electrode; <iii> another intermediate state, PTFE film is sliding apart the outer Cu electrode; <iv> another static equilibrium state.

To further verify the working mechanism of the DEL-WD-TENG, the finite element simulation (FEM) method is used to simulate the electric potential distribution, as shown in Figure 2f. When PTFE film is completely attached to Cu electrode 1 or 2, the potential difference reaches the maximum. As PTFE films gradually slide towards copper 2 or 1, the potential difference decreases, as shown in Figure 2f(ii,iii). The potential difference verified the working mechanism of the DEL-WD-TENG.

#### 2.4. Output Performance of the DEL-WD-TENG

The effect of different grid numbers ( $X$ ) on the energy conversion efficiency of the DEL-WD-TENG is studied. As shown in Figure S3, when  $X$  is 6, short circuit current ( $I_{SC}$ ) and mechanical energy conversion efficiency are the highest. When  $X$  is 4, the large area of PTFE film attached to Cu electrode increases the electrostatic adsorption and friction loss between the PTFE film and Cu electrodes, resulting in an increase in the input mechanical energy and a decrease in the mechanical energy conversion efficiency. When  $X$  is 8, the decrease in grid area leads to the decrease in adsorption between the PTFE film and the Cu electrode, which reduces the output performance of the DEL-WD-TENG. Hence,  $X$  is set as 6 in the following experiment.

The output performance and energy conversion efficiency of the DEL-WD-TENG at different rotational speeds is shown in Figure 3. When the rotational speed is lower than 400 rpm, the transferred charge of the inner WD-TENG decreases from 250 nC to 200 nC with the increase in rotational speed, as shown in Figure 3a. The corresponding charge density decreases from 25 to 20  $\mu\text{C m}^{-2}$ . The  $I_{SC}$  of the inner WD-TENG increases from 2.5 to 10  $\mu\text{A}$ , as shown in Figure 3b. The output voltage of the inner WD-TENG also decreases with the increase in rotational speed [31,32]. The decrease in transferred charge and output voltage is attributed to the increase in centrifugal force and the decrease in adsorption between the two triboelectric layers. When the rotational speed is higher than 400 rpm, as the centrifugal force increases with the increase in rotational speed, the transferred charge,  $I_{SC}$ , and output voltage of the outer WD-TENG are slightly increased, which can reach 310 nC, 38  $\mu\text{A}$ , and 3500 V, as shown in Figure 3d–f, respectively. Therefore, the DEL-WD-TENG can adapt to any rotational speed.

As shown in Figure S4, when the rotational speed is lower than 400 rpm, the outer WD-TENG has almost no output, and vice versa. Hence, this part of the output is negligible. The mechanical energy conversion efficiencies of the DEL-WD-TENG under different rotating speeds and different loads are measured, as shown in Figure 3g,h. When the rotational speed is lower than 400 rpm, the maximum energy conversion efficiency of the DEL-WD-TENG can reach 10.3%; and when rotational speed is higher than 400 rpm, the maximum energy conversion efficiency of the DEL-WD-TENG can reach 7.2%, which is still improving with the increase in rotational speed. Compared with other WD-TENGs, the mechanical energy conversion efficiency at 300 rpm is significantly improved, as shown in Figure 3i [27,31,33,34].

To test the long-term stability of the DEL-WD-TENG, a long-term operation experiment is conducted. As shown in Figure 4a, the transferred charge of the DEL-WD-TENG is relatively stable, and the total attenuation is less than 5% after more than 200 h of continuous operation (7 million cycles) at 500 rpm. Moreover, the mass of PTFE films is reduced from 1.6004 g to 1.5102 g, and the loss is only 5.6%, as shown in Figure 4b. As shown in Figure 4c and Video S1, 200 green LEDs can easily be lit by the DEL-WD-TENG at 200 rpm.

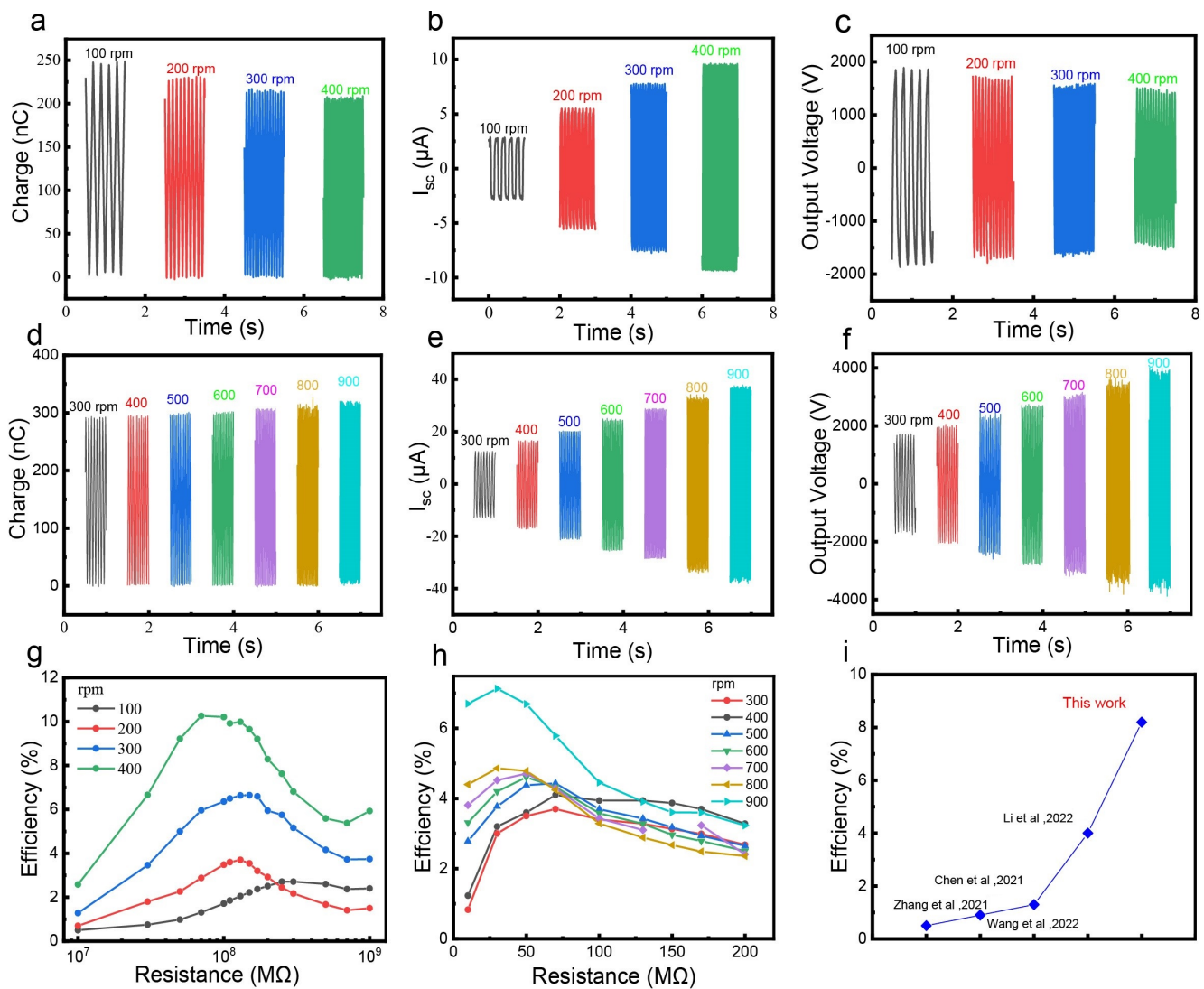


**Figure 3.** (a) Transferred charge, (b) short-circuit current, (c) and output voltage of the inner WD-TENG at different rotational speeds; (d) transferred charge, (e) short-circuit current, and (f) output voltage of the outer WD-TENG at different rotational speeds. Mechanical energy conversion efficiency of (g) the inner WD-TENG and (h) the outer WD-TENG at different rotational speeds. (i) Comparison of mechanical energy conversion efficiency of the DEL-WD-TENG with the literature at the same rotational speed [27,31,33,34].

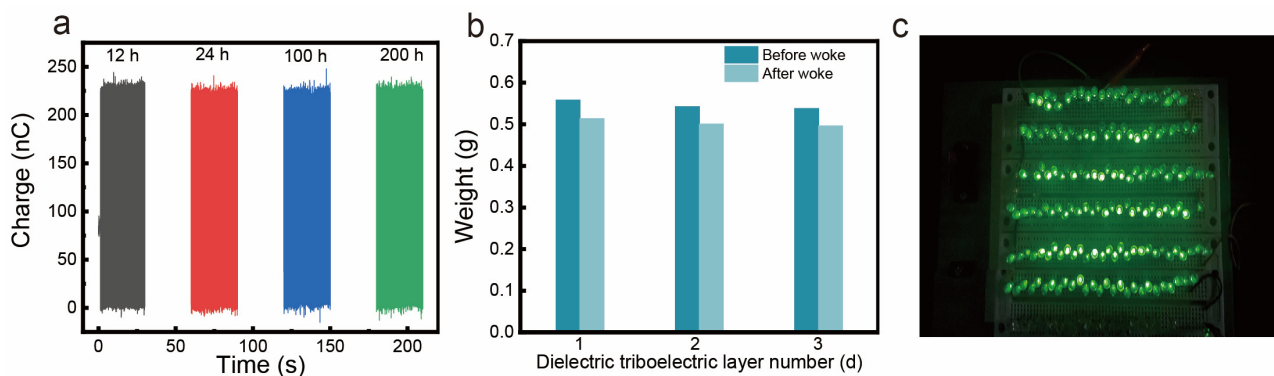


**Figure 4.** (a) Long-term stability of the DEL-WD-TENG. (b) Weight of the PTFE layer of the DEL-WD-TENG after working 200 h. (c) Two-hundred green LEDs lit by the DEL-WD-TENG after rectification at 200 rpm.

### 2.5. Demonstration of Self-Powered System

Distributed sensors play an important role in the era of Internet of things, big data, etc. Powering such a large number of distributed sensors is a challenge. Installing WD-TENGs in places with high wind speed can convert wind energy into electricity. The electric energy can be stored in capacitors through power management circuits to power sensors [35,36]. The power management circuit of the DEL-WD-TENG via a tip-tip air discharge switch is shown in Figure S5. The charging time of the capacitor at different rotational speeds is shown in Figure 5a. The higher the rotational speed, the shorter the charging time. As shown in Figure 5b and Video S2, four commercial temperature/humidity sensors can be directly driven by the DEL-TENG through the power management circuit. The DEL-WD-TENG provides a power supply curve for commercial wireless temperature sensor nodes with ZigBee wireless transmission function, as shown in Figure 5c and Video S3. When the rotational speed is 500 rpm, data transmission can be completed once every two minutes, as shown in Figure 5d. The data transmission frequency can be adjusted as required to remotely monitor the surrounding environment.

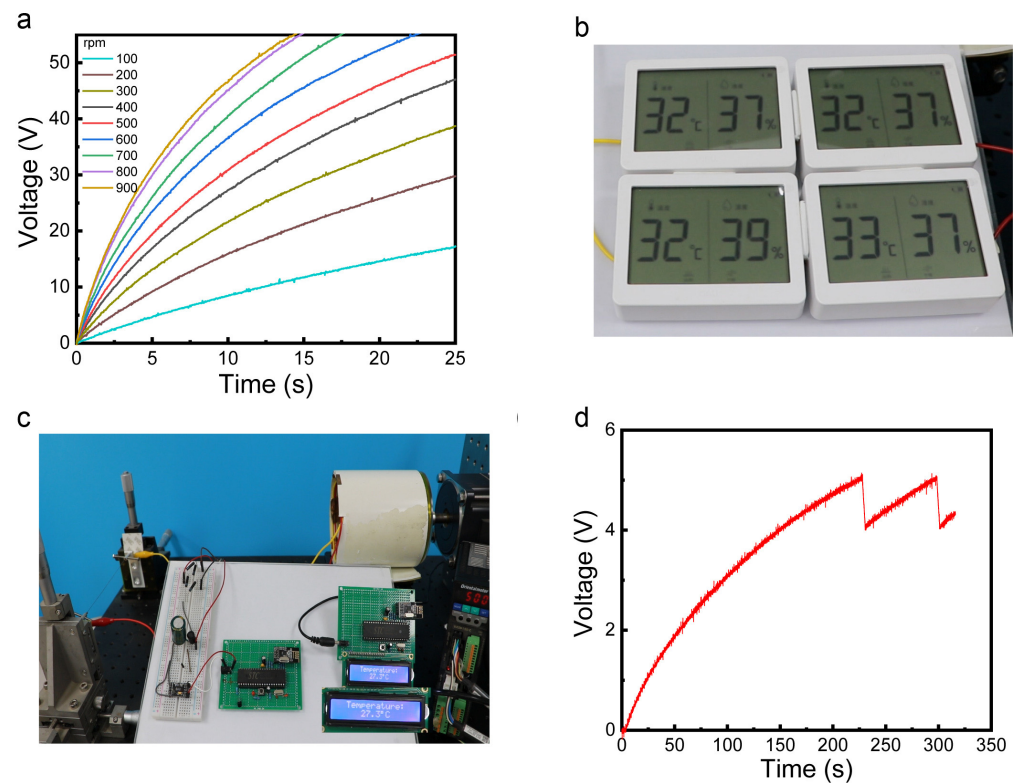


**Figure 5.** Application of the DEL-WD-TENG: (a) charging curves of the DEL-WD-TENG on capacitors at different rotational speeds; (b) photo image of the DEL-WD-TENG powering four commercial temperature and humidity sensors; (c) photo image of the wireless temperature sensor and (d) the charging and discharging curve of the wireless temperature sensor driven by the DEL-WD-TENG and power management circuit.

### 3. Conclusions

In conclusion, based on optimizing the structure and parameters of a horizontal-axis wind turbine, a DEL-WD-TENG is developed. The main interaction between the electrode and the dielectric triboelectric layer comes via the electrostatic adsorption force, which can effectively reduce frictional resistance and abrasion, improving the working life and energy conversion efficiency of the WD-TENG. When the rotational speed is lower than 400 rpm, the triboelectric layer rubs with the inner electrode layer; when the rotational speed is higher than 400 rpm, the triboelectric layer rubs with the outer electrode layer under the action of centrifugal force. The efficiency of mechanical energy to electricity of

the DEL-WD-TENG can reach 10.3%. After 7 million cycles, the transferred charge of the DEL-WD-TENG is reduced by about 5.0%, and the mass loss of the dielectric triboelectric layer is only 5.6%. The DEL-WD-TENG with low frictional resistance and high energy conversion efficiency has important application prospects in wind energy harvesting and self-powered systems.

Future research directions: increase charge density and increase the output performance of the WD-TENG, i.e., select materials with large electronegativity differences according to the triboelectric sequence to increase the transferred charges and increase the charge density by modifying the surface through polarization, charge injection, and chemical or physical aspects to produce micro–nano structures and improve output and energy conversion efficiency.

Further reduce resistance and wear: use printed circuit boards and other technologies to eliminate the geometric concave–convex structure of the electrode, reduce the resistance generated by the triboelectric layer with the electrodes, and improve energy conversion efficiency; choose a soft and dense dielectric triboelectric layer to reduce the wear and tear on the triboelectric layer.

Improve the wind energy utilization rate of the wind turbine: further improve the wind energy utilization rate by optimizing the structure of the wind turbine; continue to increase the number of layers to improve space utilization.

#### 4. Experimental Section

**Fabrication of the DEL-WD-TENG:** The wind turbine blade is a common fan blade with a diameter of 53.3 cm. The thicknesses of the Cu electrode and the PTFE film are 0.3 and 0.05 mm, respectively. We selected PVB tubes with inner diameters of 80 and 100 mm, respectively, and with a thickness of 5 mm, and used a cutting machine to cut them into a tubular structure with a length of 100 mm as the support structure of the TENG. We used a paper cutter to cut a 1 mm-thick copper sheet into 6 pieces with two dimensions of 43.5 mm × 100 mm and 51.5 mm × 100 mm, respectively, which are used as electrode layers. The 6 equally divided rectangles are glued to the outside of the PVB tube with an inner diameter of 80 mm and an inner-side diameter of 100 mm, respectively, with 3M glue. The two electrodes are separated by 1 mm, and the separated electrodes are connected and fixed on the acrylic plate as stators of the inner and outer TENG with wires. The rotor structure is drawn using the software Corel DRAW. On the rotor design drawing, we drew a circle with a size of 100 mm and three rectangles with a size of 100 mm × 3 mm, and drew three squares with a size of 3 mm × 3 mm on the circle, which are inscribed at the vertices of the congruent triangles with a diameter of 92 mm. The circles have the same center. We imported the drawing of the rotor into the laser cutting machine via Corel DRAW software; the laser cutting machine comes with the software required to automatically recognize the graphics. We selected a 3 mm thick acrylic plate, put it inside the laser cutting machine box, adjusted the cutting origin, set the power, and carried out the cutting. We glued the three cuboids obtained by cutting to the circle with acrylic glue to obtain acrylic columns distributed in congruent triangles, and we connected the other side to the flange with 3M glue as the rotor of the TENG. We used scissors to glue the 0.05-mm thick PTFE film. The PTFE film was cut into a rectangle of 65 mm × 80 mm, ultrasonically cleaned with deionized water, wiped with ethanol, and finally dried with nitrogen as a triboelectric layer. The PTFE film was then glued to the acrylic column with Kapton, and the acrylic column was placed between the two TENGs. The flange and the fan blades are connected via a coupling, supported between the bearings, and the effect of the acrylic column rotating between the two TENGs is achieved via natural wind blowing.

**Measurement of electrical signals:** All tests are performed at room temperature and with a relative humidity of about 30%. The voltage, current, and transferred charge are measured with Keithley 6514 system electrometer. The resistors used are ZX21g rotary resistance boxes and solid carbon (glass glaze) high-voltage resistors, respectively. The capacitors used are inline ceramic capacitors. Torque and rotational speed are measured

by a torque machine (Dayang Sensors LTD, DY-200. Bengbu Dayang Sensing System Engineering Co., Ltd., Bengbu, China).

**Supplementary Materials:** The following supporting information can be downloaded at: <https://www.mdpi.com/article/10.3390/nanoenergyadv3030012/s1>, Figure S1: A self-powered environmental monitoring system through harvesting wind energy by WD-TENG; Figure S2. Schematic diagram of the working mechanism of the outer WD-TENG; Figure S3. Comparison of output performance and mechanical energy conversion efficiency of DEL-WD-TENG with different grids. Electric output of the outer WD-TENG with (a) 4 grids, (b) 6 grids, and (c) 8 grids at different rotational speeds. (d) Electrical output of 4 grids, 6 grids, and 8 grids of the inner WD-TENG at different rotational speeds. Comparison of mechanical energy conversion efficiency with different grids of the (e) inner WD-TENG and (f) the outer WD-TENG; Figure S4. (a). Short-circuit current of the inner WD-TENG when rotational speed is higher than 400 rpm and (b) Short-circuit current of the outer WD-TENG when rotational speed is lower than 400 rpm; Figure S5. Power management circuit diagram of DEL-WD-TENG via a tip-tip air discharge switch. (a) Current direction when the tip-tip air discharge switch is on state, the energy transferred from the DEL-WD-TENG to the inductor. (b) Current direction when the tip-tip air discharge switch is off state, the energy transfers from the inductor to the capacitor. Video S1: Light up LEDs. Video S2: Power commercial temperature and humidity sensors. Video S3: Continuously powering wireless temperature sensor.

**Author Contributions:** D.F.: Conceptualization, visualization, validation, formal analysis, data curation, writing—original draft preparation. G.G. (Guangqin Gu): writing—review and editing, supervision, project administration, funding acquisition. W.Z.: Visualization, validation, formal analysis. C.W.: Visualization, validation, formal analysis. G.G. (Guangxiang Gu): Validation, formal analysis, data curation. B.Z.: Visualization, validation, formal analysis. G.C.: Supervision, project administration, funding acquisition. Z.D.: Supervision, project administration. All authors have read and agreed to the published version of the manuscript.

**Funding:** This research was funded by National Natural Science Foundation of China (grant number: 61974040, 52202230) and Key Research & Development and Promotion Project of Henan Province (Science and Technology Tackling Key Problems, grant number: 212102311004).

**Data Availability Statement:** The data are available upon reasonable request from the corresponding author.

**Conflicts of Interest:** The authors declare no conflict of interest.

## References

1. Dyrholm, M.; Backwell, B.; Gannoum, E.; Mapes, C.; Zhao, F. Global Wind Energy Council. *Sao Paulo Braz. Glob. Wind. Rep.* **2023**, *2023*, 27.
2. Vargas, S.A.; Esteves, G.R.T.; Maçaira, P.M.; Bastos, B.Q.; Cyrino Oliveira, F.L.; Souza, R.C. Wind power generation: A review and a research agenda. *J. Cleaner Prod.* **2019**, *218*, 850–870. [[CrossRef](#)]
3. Fan, F.; Tian, Z.; Wang, Z.L. Flexible triboelectric generator. *Nano Energy* **2012**, *1*, 328–334. [[CrossRef](#)]
4. Ren, Z.; Wu, L.; Pang, Y.; Zhang, W.; Yang, R. Strategies for effectively harvesting wind energy based on triboelectric nanogenerators. *Nano Energy* **2022**, *100*, 107522. [[CrossRef](#)]
5. Wang, S.; Mu, X.; Wang, X.; Gu, A.Y.; Wang, Z.L.; Yang, Y. Elasto-aerodynamics-driven triboelectric nanogenerator for scavenging air-flow energy. *ACS Nano* **2015**, *9*, 9554–9563. [[CrossRef](#)]
6. Sun, W.; Ding, Z.; Qin, Z.; Chu, F.; Han, Q. Wind energy harvesting based on fluttering double-flag type triboelectric nanogenerators. *Nano Energy* **2020**, *70*, 104526. [[CrossRef](#)]
7. Zhang, Y.; Fu, S.-C.Z.; Chan, K.C.; Shin, D.-M.; Chao, C.Y.H. Boosting power output of flutter-driven triboelectric nanogenerator by flexible flagpole. *Nano Energy* **2021**, *88*, 106284. [[CrossRef](#)]
8. Yang, Y.; Zhu, G.; Zhang, H.; Chen, J.; Zhong, X.; Lin, Z.H.; Su, Y.; Bai, P.; Wen, X.; Wang, Z.L. Triboelectric nanogenerator for harvesting wind energy and as self-powered wind vector sensor system. *ACS Nano* **2013**, *7*, 9461–9468. [[CrossRef](#)]
9. Seol, M.L.; Woo, J.H.; Jeon, S.B.; Kim, D.; Park, S.J.; Hur, J.; Choi, Y.K. Vertically stacked thin triboelectric nanogenerator for wind energy harvesting. *Nano Energy* **2015**, *14*, 201–208. [[CrossRef](#)]
10. Wang, Y.; Yang, E.; Chen, T.; Wang, J.; Hu, Z.; Mi, J.; Pan, X.; Xu, M. A novel humidity resisting and wind direction adapting flag-type triboelectric nanogenerator for wind energy harvesting and speed sensing. *Nano Energy* **2020**, *78*, 105279. [[CrossRef](#)]
11. Ma, P.; Zhu, H.; Lu, H.; Zeng, Y.; Zheng, N.; Wang, Z.L.; Cao, X. Design of biodegradable wheat-straw based triboelectric nanogenerator as self-powered sensor for wind detection. *Nano Energy* **2021**, *86*, 106032. [[CrossRef](#)]

12. Zhang, L.; Meng, B.; Xia, Y.; Deng, Z.; Dai, H.; Hagedorn, P.; Peng, Z.; Wang, L. Galloping triboelectric nanogenerator for energy harvesting under low wind speed. *Nano Energy* **2020**, *70*, 104477. [[CrossRef](#)]
13. Wang, Y.; Chen, T.; Sun, S.; Liu, X.; Hu, Z.; Lian, Z.; Liu, L.; Shi, Q.; Wang, H.; Mi, J.; et al. A humidity resistant and high performance triboelectric nanogenerator enabled by vortex-induced vibration for scavenging wind energy. *Nano Res.* **2021**, *15*, 3246–3253. [[CrossRef](#)]
14. Feng, Y.; Zhang, L.; Zheng, Y.; Wang, D.; Zhou, F.; Liu, W. Leaves based triboelectric nanogenerator (TENG) and TENG tree for wind energy harvesting. *Nano Energy* **2019**, *55*, 260–268. [[CrossRef](#)]
15. Li, H.; Wen, J.; Ou, Z.; Su, E.; Xing, F.; Yang, Y.; Sun, Y.; Wang, Z.L.; Chen, B. Leaf-like tengs for harvesting gentle wind energy at an air velocity as low as  $0.2 \text{ m s}^{-1}$ . *Adv. Funct. Mater.* **2023**, *33*, 2212207. [[CrossRef](#)]
16. Ren, Z.; Wang, Z.; Liu, Z.; Wang, L.; Guo, H.; Li, L.; Li, S.; Chen, X.; Tang, W.; Wang, Z.L. Energy harvesting from breeze wind ( $0.7\text{--}6 \text{ ms}^{-1}$ ) using ultra-stretchable triboelectric nanogenerator. *Adv. Energy Mater.* **2020**, *10*, 2001770. [[CrossRef](#)]
17. Chen, S.; Gao, C.; Tang, W.; Zhu, H.; Han, Y.; Jiang, Q.; Li, T.; Cao, X.; Wang, Z.L. Self-powered cleaning of air pollution by wind driven triboelectric nanogenerator. *Nano Energy* **2015**, *14*, 217–225. [[CrossRef](#)]
18. Guo, H.; Wen, Z.; Zi, Y.; Yeh, M.-H.; Wang, J.; Zhu, L.; Hu, C.; Wang, Z.L. A water-proof triboelectric-electromagnetic hybrid generator for energy harvesting in harsh environments. *Adv. Energy Mater.* **2016**, *6*, 1501593. [[CrossRef](#)]
19. Fan, X.; He, J.; Mu, J.; Qian, J.; Zhang, N.; Yang, C.; Hou, X.; Geng, W.; Wang, X.; Chou, X. Triboelectric-electromagnetic hybrid nanogenerator driven by wind for self-powered wireless transmission in Internet of Things and self-powered wind speed sensor. *Nano Energy* **2020**, *68*, 104319. [[CrossRef](#)]
20. Fu, X.; Xu, S.; Gao, Y.; Zhang, X.; Liu, G.; Zhou, H.; Lv, Y.; Zhang, C.; Wang, Z.L. Breeze-wind-energy-powered autonomous wireless anemometer based on rolling contact-electrification. *ACS Energy Lett.* **2021**, *6*, 2343–2350. [[CrossRef](#)]
21. Liu, S.; Li, X.; Wang, Y.; Yang, Y.; Meng, L.; Cheng, T.; Wang, Z.L. Magnetic switch structured triboelectric nanogenerator for continuous and regular harvesting of wind energy. *Nano Energy* **2021**, *83*, 105851. [[CrossRef](#)]
22. Luo, Y.; Chen, P.; Cao, L.N.Y.; Xu, Z.; Wu, Y.; He, G.; Jiang, T.; Wang, Z.L. Durability improvement of breeze-driven triboelectric-electromagnetic hybrid nanogenerator by a travel-controlled approach. *Adv. Funct. Mater.* **2022**, *32*, 2205710. [[CrossRef](#)]
23. Wang, Y.; Yu, X.; Yin, M.; Wang, J.; Gao, Q.; Yu, Y.; Cheng, T.; Wang, Z.L. Gravity triboelectric nanogenerator for the steady harvesting of natural wind energy. *Nano Energy* **2021**, *82*, 105740. [[CrossRef](#)]
24. Xi, Y.; Guo, H.; Zi, Y.; Li, X.; Wang, J.; Deng, J.; Li, S.; Hu, C.; Cao, X.; Wang, Z.L. Multifunctional teng for blue energy scavenging and self-powered wind-speed sensor. *Adv. Energy Mater.* **2017**, *7*, 1602397. [[CrossRef](#)]
25. Zhang, C.; Liu, Y.; Zhang, B.; Yang, O.; Yuan, W.; He, L.; Wei, X.; Wang, J.; Wang, Z.L. Harvesting wind energy by a triboelectric nanogenerator for an intelligent high-speed train system. *ACS Energy Lett.* **2021**, *6*, 1490–1499. [[CrossRef](#)]
26. Li, S.; Wang, S.; Zi, Y.; Wen, Z.; Lin, L.; Zhang, G.; Wang, Z.L. Largely improving the robustness and lifetime of triboelectric nanogenerators through automatic transition between contact and noncontact working states. *ACS Nano* **2015**, *9*, 7479–7487. [[CrossRef](#)]
27. Chen, P.; An, J.; Shu, S.; Cheng, R.; Nie, J.; Jiang, T.; Wang, Z.L. Super-durable, low-wear, and high-performance fur-brush triboelectric nanogenerator for wind and water energy harvesting for smart agriculture. *Adv. Energy Mater.* **2021**, *11*, 2003066. [[CrossRef](#)]
28. Yong, S.; Wang, J.; Yang, L.; Wang, H.; Luo, H.; Liao, R.; Wang, Z.L. Auto-switching self-powered system for efficient broad-band wind energy harvesting based on dual-rotation shaft triboelectric nanogenerator. *Adv. Energy Mater.* **2021**, *11*, 2101194. [[CrossRef](#)]
29. Jiang, H.; Li, Y.; Cheng, Z. Performances of ideal wind turbine. *Renew. Energy* **2015**, *83*, 658–662. [[CrossRef](#)]
30. Wang, S.; Xie, Y.; Niu, S.; Lin, L.; Wang, Z.L. Freestanding triboelectric-layer-based nanogenerators for harvesting energy from a moving object or human motion in contact and non-contact modes. *Adv. Mater.* **2014**, *26*, 2818–2824. [[CrossRef](#)]
31. Zhang, W.; Gu, G.; Shang, W.; Luo, H.; Wang, T.; Zhang, B.; Cui, P.; Guo, J.; Yang, F.; Cheng, G.; et al. A general charge compensation strategy for calibrating the voltage of a triboelectric nanogenerator measured by a capacitive circuit. *Nano Energy* **2021**, *86*, 106056. [[CrossRef](#)]
32. Zhang, W.; Gu, G.; Qin, H.; Li, S.; Shang, W.; Wang, T.; Zhang, B.; Cui, P.; Guo, J.; Yang, F.; et al. Measuring the actual voltage of a triboelectric nanogenerator using the non-grounded method. *Nano Energy* **2020**, *77*, 105108. [[CrossRef](#)]
33. Wang, Y.; Li, X.; Yu, X.; Zhu, J.; Shen, P.; Wang, Z.L.; Cheng, T. Driving-torque self-adjusted triboelectric nanogenerator for effective harvesting of random wind energy. *Nano Energy* **2022**, *99*, 107389. [[CrossRef](#)]
34. Li, X.; Cao, Y.; Yu, X.; Xu, Y.; Yang, Y.; Liu, S.; Cheng, T.; Wang, Z.L. Breeze-driven triboelectric nanogenerator for wind energy harvesting and application in smart agriculture. *Appl. Energy* **2022**, *306*, 117977. [[CrossRef](#)]
35. Qin, H.; Gu, G.; Shang, W.; Luo, H.; Zhang, W.; Cui, P.; Zhang, B.; Guo, J.; Cheng, G.; Du, Z. A universal and passive power management circuit with high efficiency for pulsed triboelectric nanogenerator. *Nano Energy* **2020**, *68*, 104372. [[CrossRef](#)]
36. Shang, W.; Gu, G.; Zhang, W.; Luo, H.; Wang, T.; Zhang, B.; Guo, J.; Cui, P.; Yang, F.; Cheng, G. Rotational pulsed triboelectric nanogenerators integrated with synchronously triggered mechanical switches for high efficiency self-powered systems. *Nano Energy* **2021**, *82*, 105725. [[CrossRef](#)]

**Disclaimer/Publisher’s Note:** The statements, opinions and data contained in all publications are solely those of the individual author(s) and contributor(s) and not of MDPI and/or the editor(s). MDPI and/or the editor(s) disclaim responsibility for any injury to people or property resulting from any ideas, methods, instructions or products referred to in the content.